Dielectronic recombination of Mg^{2+}, P^{5+}, and Cl^{7+}

A. H. Moussa
Department of Physics, Ain Shams University, Cairo, Egypt
and Department of Physics, University of Connecticut, Storrs, Connecticut 06268

H. H.Ramadan and Y.n
Department of Physics, University of Connecticut, Storrs, Connectocut 06268
(Received 2 March 1988)

Dielectronic recombination (DR) cross sections and rate coefficients are calculated for the Ne-like Mg^{2+}, P^{5+}, and Cl^{7+} in which L-shell excitations are involved during the initial resonance capture. The result on P^{5+} is consistent with the first direct DR experiment of the $\Delta n_t \neq 0$ mode carried out recently by P. F. Dittner *et al.* Multiple Auger channels complicate the dependence of the cross sections on principal quantum number and nuclear charge. Rapid decrease in the rate coefficient with decreasing atomic number was found, except at very low temperature, where this trend is reversed.

I. INTRODUCTION

Much theoretical work on dielectronic recombination (DR) has been reported in recent years[1], but direct DR experiments have proven to be much harder to carry out because of extremely small cross sections, and its signature requires usually some type of coincidence measurements. All the presently available direct DR measurements[2-5] involve initial intrashell excitation ($\Delta n_t = 0$) and simultaneous capture of the incoming electron to high-Rydberg states (HRS), followed by stabilizing radiative decays. Because of weak binding of these HRS electrons, the corresponding cross sections are extremely sensitive to a small external field perturbation.[6]

On the other hand, the initial intershell excitation of the type (K-LL), (L-MM), etc. ($\Delta n_t \neq 0$) has been observed, only indirectly, in high-energy ion-atom collisions[7-9] [resonant transfer excitation (RTE)] and in some plasma experiments.[10-13] In view of the importance of DR in astrophysical and laboratory plasmas, it is desirable to test the DR theory[1] in the $\Delta n_t \neq 0$ mode, where external perturbations have a minimal effect. An attempt[14] was made earlier to directly measure the DR cross section for Cl^{7+}; the Ne-like ion was chosen because it allowed only the $\Delta n_t \neq 0$ mode. But the background counts were too high to extract meaningful cross-section data. However, a more recent experiment[14] on P^{5+} showed a distinct peak at the expected electron-beam energy and of correct magnitude.

Detailed theoretical data on the DR cross section are available[15-18] for Cl^{7+} and Mo^{32+} and on the rates[19] for Ar^{8+}, Fe^{16+}, and Mo^{32+}, all of the Ne isoelectronic sequence. But extrapolation to lighter ions using these data was difficult because the cross section decreases very rapidly as the nuclear core charge Z_c decreases toward $Z_c = 11$. Furthermore, the usual Z scaling of the Auger and radiative transition probabilities is badly broken for Mg^{2+}. In fact, we were able to obtain the cross section for P^{5+} from the Cl^{7+} data by extrapolation only to within an accuracy of $\pm 30\%$, while a more accurate result was needed to interpret the experimental data. The main purpose of the present calculation was to provide this needed improvement and also to carry out a detailed study of the effect of electron correlation for low-charge states. As the correlation effect becomes relatively stronger with decreasing Z_c, not only the level structures change from the Coulomb-scaled pattern but some resonances also acquire additional Auger channels. This has a drastic effect on the HRS contribution.

II. PRELIMINARY DISCUSSION

The DR processes of interest here are described as

$$\underset{e_c l_c + 1s^2 2s^2 2p^6}{e^- + P^{5+}} \rightarrow \underset{1s^2 2s^2 2p^5 n_1 l_1 n_2 l_2}{(P^{4+})^{**}} \rightarrow \underset{1s^2 2s^2 2p^6 n_1 l_1 + \gamma}{(P^{4+})^{*} + \gamma} \qquad (1)$$

$$(i) \qquad (d) \qquad (f)$$

and similarly for Mg^{2+} and Cl^{+7}. The $2s$ electron excitation as well as $1s$ excitation is also possible, but its contribution is small ($\lesssim 2\%$) and we neglect it in the following. The cross section is defined[1] in the isolated resonance approximation by

$$\sigma^{\mathrm{DR}}(i, l_c \rightarrow d \rightarrow f) = \frac{4\pi\tau_0}{e_c(\mathrm{Ry})} V_a(i, l_c \rightarrow d)\omega(d \rightarrow f)\tilde{\delta}(e_c, E_d)(\pi a_0^2) , \qquad (2)$$

where

$$V_a(i, l_c \rightarrow d) = \frac{g_d}{2g_i} A_a(d \rightarrow i, l_c)$$

is the initial excitation-capture probability (in sec^{-1}),

$$g_d = \hat{L}\hat{S} ,$$

with $\hat{L} = 2L + 1$, etc.,

$$g_i = 1 ,$$

in our case of closed-shell target ions,

$$\omega(d \to f) = \frac{A_r(d \to f)}{\Gamma(d)}$$

is the partial fluorescence yield,

$$\tilde{\delta}(E, E_d) = \left[\frac{\Gamma}{2\pi} \right] \frac{1}{(E - E_d)^2 + \Gamma^2/4}, \quad \int \tilde{\delta}\, dE = 1$$

and

$$\Gamma(d) = \sum_{i', l_c'} A_a(d \to i', l_c') + \sum_{f'} A_r(d \to f') \equiv \Gamma_a + \Gamma_r ,$$

where A_a and A_r are the Auger and radiative transition probabilities, respectively. We further have

$$\omega(d) = \sum_f \omega(d \to f) = \Gamma_r(d)/\Gamma(d) ,$$

which is the fluorescence yield of the state (d). The total cross section is defined, from (2), as

$$\sigma_{\text{tot}}^{\text{DR}}(i) = \sum_{d, l_c, f} \sigma^{\text{DR}}(i, l_c \to d \to f) . \tag{3}$$

These quantities are evaluated using nonrelativistic Hartree-Fock wave functions and in LS coupling. For details of the procedure adopted here, we refer to a review article.[1] To simplify the presentation of σ^{DR}, we further define[1] an energy-averaged cross section over the bin Δe_c as

$$\bar{\sigma}^{\text{DR}} \equiv \frac{1}{\Delta e_c} \int_{e_c - \Delta e_c/2}^{e_c + \Delta e_c/2} \sigma^{\text{DR}}(e_c')\, de_c' , \tag{4}$$

where Δe_c is arbitrarily chosen and we chose the value $\Delta e_c = 0.1$ Ry throughout this paper.

In general, there are many intermediate resonance states (d), in fact, a double infinity of states, which contribute to the total cross section $\sigma_{\text{tot}}^{\text{DR}}$ and rate coefficients $\alpha_{\text{tot}}^{\text{DR}}$. However, previous experience has shown that only a small number (100–200) of low-lying states require careful study. Contributions from the rest of the states can then be estimated using the n- and Z- scaling properties of A_a and A_r. In the present case, the Cl^{7+} data[15] already provide a rough information on the dominant intermediate states. As will be seen below, however, some states which were negligible in Cl^{7+} turned out to be quite important in P^{5+} and Mg^{2+}.

The DR rate α^{DR} is defined by a thermal average of σ^{DR} over the Maxwell distribution of electron velocities,

$$\alpha^{\text{DR}}(i, l_c \to d) = \left[\frac{4\pi \mathcal{R}}{k_B T_e} \right]^{3/2} e^{-(e_c/k_B T_e)} a_0^3 \times V_a(i, l_c \to d)\, \omega(d) . \tag{5}$$

Incidentally, the cross sections for resonant collisional excitation (RE) process can be expressed as

$$\sigma^{\text{RE}}(i, l_c \to d \to j, l_c') = \frac{4\pi\tau_0}{e_c(\text{Ry})} V_a(i, l_c \to d)\, \xi(d \to j, l_c') \times \tilde{\delta}(e_c, E_d)(\pi a_0^2) , \tag{6}$$

where

$$\xi(d \to j, l_c') = \frac{A_a(d \to j, l_c')}{\Gamma(d)}$$

is the partial Auger yield. Note that, since $A_a(d \to j, l_c')$ are already contained in $\Gamma(d)$ for $\omega(d)$ and $\xi(d)$, the information contents of σ^{DR} and σ^{RE} is nearly identical. On the other hand, in general, $\xi \gg \omega$, so that $\sigma^{\text{RE}} \gg \sigma^{\text{DR}}$, which makes the detection of Auger electrons in the RE process more attractive than the x rays detected in DR.

We divide the intermediate resonance states (d) of the process (1) into three different classes, based on the numbers of available Auger channels which contribute to Γ_a. Such a classification is useful in estimating the HRS contributions by extrapolation. For incident energies below the $2p^5 3p$ threshold, we have the following possible Auger channels: $i' = i = 2p^6$, $i' = i_1 = 2p^5 3s$, and $i' = i_2 = 2p^5 3p$. Thus class A contains those intermediate states with $\Gamma_a = \Gamma_a(d \to i)$ only; class B with both i and i_1; and class C with i, i_1, and i_2. Obviously, as the number of terms (i_1 or i_2) in $\Gamma_a(d)$ increases, $\omega(d)$ and σ^{DR} will decrease, sometimes drastically. Since the electron correlation is relatively stronger in Mg^{2+} than in P^{5+} and Cl^{7+}, we expect for different ions some rearrangements of resonance levels into different classes in such a way as to increase the number of Auger channels as Z_c decreases.

The HRS contribution ($n \geq 2l$) is estimated by assuming an n^{-3} scaling behavior. For high enough n, $n \geq 2l$, we expect the n dependence of Γ_a to be

$$\Gamma_a \sim g/n^3 .$$

(n-independent part is not present for the Ne- like ionic targets and thus omitted.)

With the strong $3s \to 2p$ and $3d \to 2p$ radiative transitions in Γ_r, which are independent of n, we also have,[1] in general,

$$\Gamma_r = a + b/n^3 .$$

In heavier ions, the HRS electron contribution b/n^3 can be very large.

For ready comparison of the cross sections for different ions, we further define the energy-integrated cross section S by

$$S \equiv \int \sigma\, de_c \equiv \sum_d \bar{\sigma}(\Delta e_c) ,$$

which is independent of Δe_c.

III. RESULTS

We summarize in Table I our calculations of $\bar{\sigma}^{\text{DR}}$ for all three ions, where the resonant states with their energies in rydbergs and class assignments are indicated. Obviously, whenever the class for a given state changes as

TABLE I. σ^{DR} vs e_c(Ry) for Mg^{2+}, P^{5+}, and Cl^{7+} in units of 10^{-20} cm^2, and $\Delta e_c = 0.1$ Ry. Class A denotes those intermediate states with only one Auger channel $d \rightarrow i = 2p^6$ allowed by energy conservation; class B with two Auger channels i and $i_1 = 2p^5 3s$; and class C for i, i_1, and $i_2 = 2p^5 3p$. The $(1s^2 2s^2 p^5)$ core is assumed in the designation of the intermediate resonance states (d). Energies for the various ionization thresholds ($n \rightarrow \infty$ limit) may also be read off the table.

	Mg^{2+}		P^{5+}		Cl^{7+}	
d	e_c	$\bar{\sigma}^{DR}$	e_c	$\bar{\sigma}^{DR}$	e_c	$\bar{\sigma}^{DR}$
$3s3s$	2.56-A	0.140	4.85-A	0.333	6.60-A	0.703
$3s4s$	3.31-A	0.208	7.76-A	0.291	11.05-A	0.429
$3s5s$	3.56-A	0.167	8.76-A	0.197	12.82-A	0.286
$n \geq 6$	3.72–3.84	1.65	9.07–9.92	1.36	13.69–15.37	1.91
$3s3p$	2.87-A	0.471	5.57-A	1.21	7.59-A	0.948
$3s4p$	3.43-A	0.349	7.84-A	0.474	11.49-A	0.323
$3s5p$	3.61-A	0.286	8.67-A	0.271	13.02-A	0.274
$3s6p$	3.66-A	0.251	9.09-A	0.209	13.80-A	0.252
$n \geq 7$	3.74–3.84	7.32	9.27–9.92	6.74	14.16–15.37	6.94
$3s3d$	3.32-A	1.04	6.75-A	8.13	9.23-A	15.4
$3s4d$	3.56-A	0.925	8.21-A	3.83	12.04-A	5.44
$3s5d$	3.67-A	0.798	8.85-A	2.47	13.28-A	2.95
$3s6d$	3.72-A	0.741	9.16-A	1.84	13.94-A	1.91
7–20	3.75–3.83	7.76	9.34–9.86	10.8	14.30–15.18	9.01
21–40	3.83–3.84	4.74	9.86–9.90	4.03	15.19–15.27	1.96
41–60	3.84	1.64	9.90–9.91	1.08	15.27–15.29	0.225
$n \geq 61$	3.84	1.60	9.91–9.92	0.928	15.29–15.37	0.347
$3s4f$	3.58-A	0.810	8.32-A	2.79	12.24-A	3.65
$3s5f$	3.68-A	0.741	8.91-A	2.09	13.38-A	3.02
$3s6f$	3.73-A	0.660	9.22-A	1.81	14.00-A	2.36
7–20	3.76–3.83	3.75	9.40–9.85	10.4	14.36–15.24	11.3
21–40	3.83–3.84	0.701	9.86–9.90	2.25	15.25–15.33	2.14
41–60	3.84	0.142	9.90–9.91	0.476	15.33–15.35	0.444
$n \geq 61$	3.84	0.115	9.91–9.92	0.387	15.35–15.37	0.360
$3s5g$	3.68-A	0.133	8.91-A	0.998	13.40-A	1.45
$3s6g$	3.73-A	0.139	9.23-A	0.944	14.01-A	1.32
$3s7g$	3.76-A	0.0923	9.41-A	0.694	14.37-A	0.972
$n \geq 8$	3.78–3.84	0.303	9.53–9.92	2.72	14.60–15.37	3.81
$3s6h$	3.73-A	0.0021	9.23-A	0.058	14.01-A	0.0812
$3s7h$	3.76-A	0.0013	9.41-A	0.0354	14.37-A	0.0496
$3s8h$	3.78-A	0.0009	9.53-A	0.0237	14.60-A	0.0332
$n \geq 9$	3.79–3.84	0.0031	9.62–9.92	0.0835	14.76–15.37	0.112
$3p4s$	3.75-A	0.280	8.40-A	0.315	12.24-A	0.441
$3p5s$	4.01-B	0.003 50	9.42-A	0.139	14.00-A	0.195
$3p6s$	4.06-B	0.002 24	9.91-A	0.0890	14.87-A	0.125
$3p7s$	4.09-B	0.001 41	10.40-B	0.0180	15.23-A	0.0252
$n \geq 8$	4.11–4.27	0.574	10.68–10.80	0.142	15.46–16.54-B	1.99
$3p3p$	3.32-A	0.138	6.50-A	0.190	8.85-A	0.289
$3p4p$	3.86-B	0.008	8.69-A	0.300	12.66-A	0.419
$3p5p$	4.05-B	0.007	9.55-A	0.176	14.20-A	0.246
$3p6p$	4.10-B	0.0041	9.98-B	0.0512	14.79-A	0.0717
$3p7p$	4.13-B	0.0026	10.16-B	0.0392	15.15-A	0.005 49
$n \geq 8$	4.15–4.27	1.25	10.28–10.80	2.49	15.38–16.54-B	3.49
$3p3d$	3.74-A	1.33	7.59-A	12.3	10.37-A	23.5
$3p4d$	4.00-B	0.270	9.08-A	4.43	13.21-A	9.04
$3p5d$	4.11-B	0.125	9.73-A	2.32	14.46-A	4.35
$3p6d$	4.16-B	0.090	10.04-B	0.424	15.12-B	0.922
$3p7d$	4.19-B	0.0725	10.22-B	0.279	15.48-B	1.16
$3p8d$	4.21-B	0.0626	10.34-B	0.200	15.71-B	0.637
$n \geq 9$	4.22–4.27	3.19	10.43–10.80	5.14	15.87–16.54	6.49

TABLE I. (*Continued*).

	Mg^{2+}		P^{5+}		Cl^{7+}	
d	e_c	$\bar{\sigma}^{DR}$	e_c	$\bar{\sigma}^{DR}$	e_c	$\bar{\sigma}^{DR}$
$3p4f$	4.03-*A*	0.0640	9.23-*A*	2.52	13.41-*A*	4.64
$3p5f$	4.11-*B*	0.0530	9.79-*A*	1.15	14.56-*A*	2.49
$3p6f$	4.16-*B*	0.004 77	10.10-*B*	0.188	15.17-*A*	1.55
$3p7f$	4.19-*B*	0.003	10.28-*B*	0.132	15.53-*A*	1.04
$3p8f$	4.21-*B*	0.002 01	10.40-*B*	0.102	15.76-*B*	0.189
$3p9f$	4.22-*B*	0.001 41	10.50-*B*	0.0841	15.94-*B*	0.145
$3p10f$	4.23-*B*	0.001 03	10.55-*B*	0.0724	16.05-*B*	0.115
$n \geq 11$	4.24–4.27	0.321	10.60–10.80	1.21	16.14–16.54	1.62
$3p5g$	4.13-*B*	0.007 30	9.80-*B*	0.106	14.58-*A*	0.874
$3p6g$	4.18-*B*	0.004 22	10.11-*B*	0.0615	15.18-*A*	0.506
$3p7g$	4.21-*B*	0.002 66	10.29-*B*	0.0387	15.54-*A*	0.319
$3p8g$	4.23-*B*	0.001 78	10.41-*B*	0.0259	15.77-*B*	0.0480
$3p6h$	4.18-*B*	0.000 051	10.12-*B*	0.003 16	15.19-*A*	0.0888
$3p7h$	4.21-*B*	0.000 032	10.30-*B*	0.001 99	15.55-*B*	0.0161
$3d4s$	4.25-*B*	0.0450	9.54-*A*	5.74	13.78-*A*	10.3
$3d5s$	4.51-*C*	0.007 50	10.56-*B*	1.69	15.54-*B*	2.25
$3d6s$	4.63-*C*	0.003 99	11.04-*B*	0.0666	16.40-*B*	0.812
$3d7s$	4.66-*C*	0.002 51	11.22-*C*	0.0419	16.89-*C*	0.0557
$n \geq 8$	4.68–4.78	0.665	11.34–11.90	2.09	17.19–18.08	4.40
$3d4p$	4.36-*C*	0.0440	9.83-*A*	12.1	14.20-*A*	19.8
$3d5p$	4.56-*C*	0.0450	10.69-*B*	4.68	15.74-*B*	7.23
$3d6p$	4.65-*C*	0.0370	11.11-*C*	0.431	16.51-*B*	5.82
$3d7p$	4.68-*C*	0.0372	11.29-*C*	0.370	16.96-*C*	0.627
$3d8p$	4.70-*C*	0.0368	11.41-*C*	0.361	17.24-*C*	0.600
9–20	4.71–4.77	0.418	11.50–11.84	3.72	17.42–17.90	5.64
21–40	4.78	0.539	11.84–11.89	3.55	17.91–17.99	4.83
41–60	4.78	0.368	11.89–11.90	1.65	17.99–18.01	2.10
$n \geq 61$	4.78	0.812	11.90	2.40	18.01–18.08	2.58
$3d3d$	4.22-*B*	0.664	8.75-*A*	14.4	11.97-*A*	30.6
$3d4d$	4.50-*C*	0.0277	10.21-*B*	6.97	14.74-*A*	24.8
$3d5d$	4.62-*C*	0.0437	10.87-*C*	1.79	16.00-*B*	11.6
$3d6d$	4.68-*C*	0.0543	11.21-*C*	2.89	16.65-*C*	6.09
$3d7d$	4.71-*C*	0.0527	11.39-*C*	2.75	17.04-*C*	6.13
$3d8d$	4.73-*C*	0.0518	11.51-*C*	2.64	17.29-*C*	5.82
9–20	4.74–4.77	0.562	11.60–11.84	26.8	17.46–17.94	54.0
21–40	4.78	0.597	11.84–11.89	25.5	17.95–18.03	34.7
41–60	4.78	0.243	11.89–11.90	10.4	18.03–18.05	16.4
$n \geq 61$	4.78	1.62	11.90	11.3	18.05–18.08	15.2
$3d4f$	4.53-*C*	0.001 40	10.33-*B*	4.96	14.94-*A*	37.8
$3d5f$	4.63-*C*	0.001 20	10.92-*C*	0.0896	16.09-*B*	13.3
$3d6f$	4.69-*C*	0.001 50	11.24-*C*	0.113	16.71-*C*	0.494
$3d7f$	4.72-*C*	0.000 945	11.42-*C*	0.0701	17.08-*C*	0.563
$3d8f$	4.74-*C*	0.000 633	11.54-*C*	0.0685	17.31-*C*	0.474
$n \geq 9$	4.75–4.78	0.134	11.63–11.90	2.75	17.48–18.08	14.3
$3d5g$	4.64-*C*	0.001 99	10.94-*C*	0.009 20	16.11-*B*	3.20
$3d6g$	4.69-*C*	0.002 80	11.25-*C*	0.005 32	16.72-*C*	0.007 66
$3d6h$	4.69-*C*	0.000 046 5	11.19-*C*	0.0015	16.72-*C*	0.002 16

Z_c decreases, a large reduction in the cross section was observed. Thus, in the n extrapolation for the contribution of HRS, one has to be certain that higher-class states of the particular n sequence do not appear beyond some n values, where the n extrapolation is made. The cross section for P^{5+} is plotted in Fig. 1. The general feature of the cross sections for Mg^{2+} and Cl^{7+} is similar to that of P^{5+}. In particular, we note that the large peak near the

ionization threshold ($e_c \sim 12$ Ry) for $1s^2 2s^2 2p^5$ comes from the large-n contribution, and is present in general in all the DR cross sections. One exception is the case in which n-independent Auger decay channels are present, so that, for high n, $\Gamma_a \sim f + g/n^3$; the HRS contribution is then severely suppressed and the threshold peak disappears. An example of this was seen in the $\Delta n_t \neq 0$ transitions in Li-like ions[1] (Si^{11+} and S^{13+}, e.g.,). On the other hand, the high-n peak is more pronounced in the $\Delta n_t = 0$ transitions, as seen[6] in Mg^+ and Ca^+. Of course, these HRS contributions will be especially sensitive to external field perturbations.

The rate coefficients for Mg^{2+}, P^{5+} and Cl^{7+} are shown in Fig. 2 as functions of $k_B T_e$. The temperature dependence of the rate coefficient is as expected; it is dominated by the $\exp(-e_c/k_B T_e)$ factor at low temperature and by the $(k_B T_e)^{-3/2}$ factor at high temperature. However, the behavior at a very low temperature was quite surprising in that the rates for lower Z_c ions become larger; in fact, $\alpha^{DR}(P^{5+}) > \alpha^{DR}(Cl^{7+})$ for $k_B T_e < 4.5$ Ry and $\alpha^{DR}(Mg^{2+}) > \alpha^{DR}(P^{5+})$ for $k_B T_e < 1.5$ Ry. Figure 3 shows the maximum rate coefficients for the ten-electron ions calculated at scaled temperatures $k_B T_e \sim Z^2$. The figure includes the earlier results[19] for Ar^{8+}, Fe^{16+}, and Mo^{32+}.

We now compare the overall magnitude of the cross sections for the three ions of interest here. Our calculation gives

$$S(Mg^{2+}) = 0.53 \times 10^{-19} \text{ cm}^2 \text{ Ry} ,$$

$$S(P^{5+}) = 2.6 \times 10^{-19} \text{ cm}^2 \text{ Ry} ,$$

$$S(Cl^{7+}) = 4.9 \times 10^{-19} \text{ cm}^2 \text{ Ry} ,$$

thus

$$S(Mg^{2+})/S(P^{5+}) \sim 0.20 ,$$

$$S(P^{5+})/S(Cl^{7+}) \sim 0.53 .$$

Preliminary measurement[14] of the cross section for P^{5+} is consistent with the above, both in magnitude and in relation to that for Cl^{7+}. However, a more detailed measurement is yet to be carried out.

It is also of interest to examine whether the relative magnitude of S may be understood from an approximate Z scaling of σ and S. That is,[1] in terms of an effective charge Z, we have

$$A_r \sim \omega \sim Z^4 \quad \text{for } \Gamma_r \ll \Gamma_a ,$$

$$A_a \sim \Gamma_a \sim Z^0, \quad e_c \sim Z^2 ,$$

and thus

$$\sigma^{DR} \sim \frac{1}{Z^2} Z^0 Z^4 \sim Z^2 .$$

The dependence $(k_c a_0)^2 \sim Z^2$ is used for the present case of the $\Delta n_t \neq 0$ mode. For ions of low degrees of ionization, it was found earlier that a form $Z \sim \sqrt{Z_c Z_I}$ works well in determining the Z dependence of A_r, where Z_I is

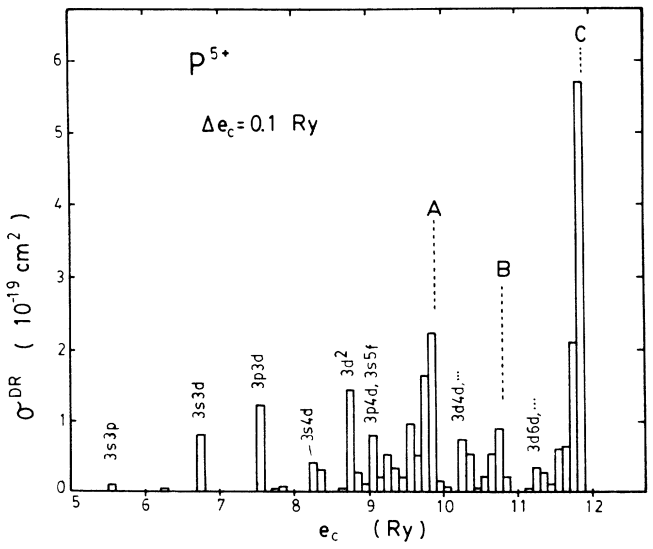

FIG. 1. $\bar{\sigma}^{DR}$ vs e_c(Ry) for P^{5+} in units of 10^{-20} cm^2, and $\Delta e_c = 0.1$ Ry. $\bar{\sigma}^{DR}$ for Mg^{2+} and Cl^{7+} exhibit a similar behavior.

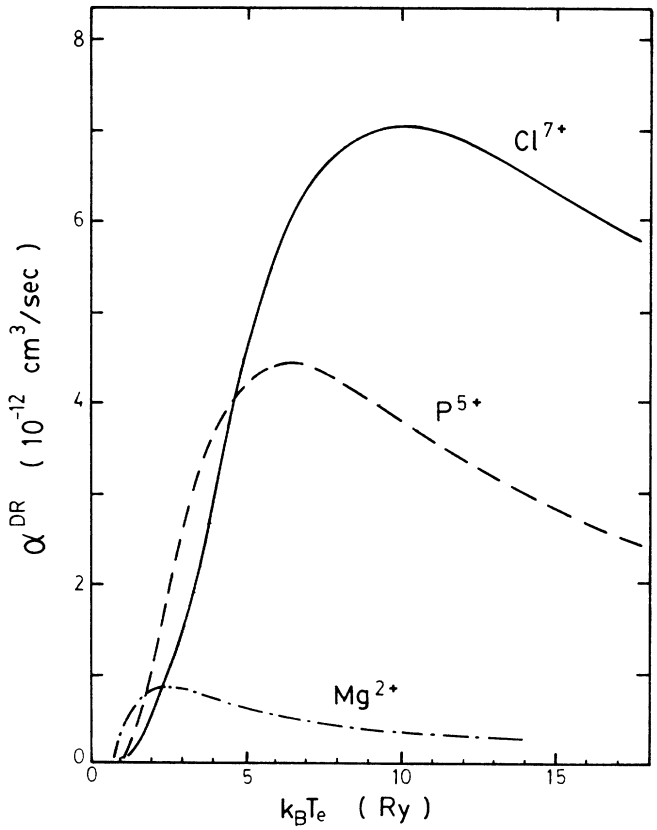

FIG. 2. α^{DR} vs $(k_B T_e)$ for Mg^{2+}, P^{5+}, and Cl^{7+} in units of 10^{-12} cm^3 sec^{-1}. Note the reversal in relative magnitudes at low temperature.

the asymptotic charge of the initial ions. [For $Z_I \geq Z_c/2$, $Z \sim (Z_I + Z_c)/2$ works better.] We thus have $Z(Mg^{2+}) = 4.9$, $Z(P^{5+}) = 8.7$, and $Z(Cl^{7+}) = 11$. This in turn predicts

$$S(Mg^{2+})/S(P^{5+}) = 24/75 \sim 0.32 ,$$

$$S(P^{5+})/S(Cl^{7+}) = 75/119 \sim 0.63 ,$$

which are in reasonable agreement with the actual calculation. We also note that the temperature $k_B T_e$ at which the rate is maximum roughly scales as Z^2. (We caution, however, that an effective charge Z which is valid for bound state energies may not be valid for A_a or A_r, and vice versa.)

Figure 3 summarizes the maximum rates α^{DR} and the corresponding temperature $k_B T_e$, all as functions of the nuclear core charge Z_c. The sharp decrease of α^{DR} at low Z_c is apparent. From the behavior of α^{DR} in this figure, we suggest that the experimentally optimum ions (with not too high Z_c but large σ^{DR}) may be those between $Z_c = 20$–26 (Ca–Fe). Note that S for ions in this region will be two to three times larger than that for Cl.

Finally, cross sections for other resonant processes in electron-ion collisions can be estimated using the data presented here, as indicated for resonance excitation process in (6). Sample data are given in Appendix A and Table II in which the relevant quantities needed for σ^{DR}, α^{DR}, and possibly for σ^{RE}, are presented for three intermediate states which are chosen for illustration.

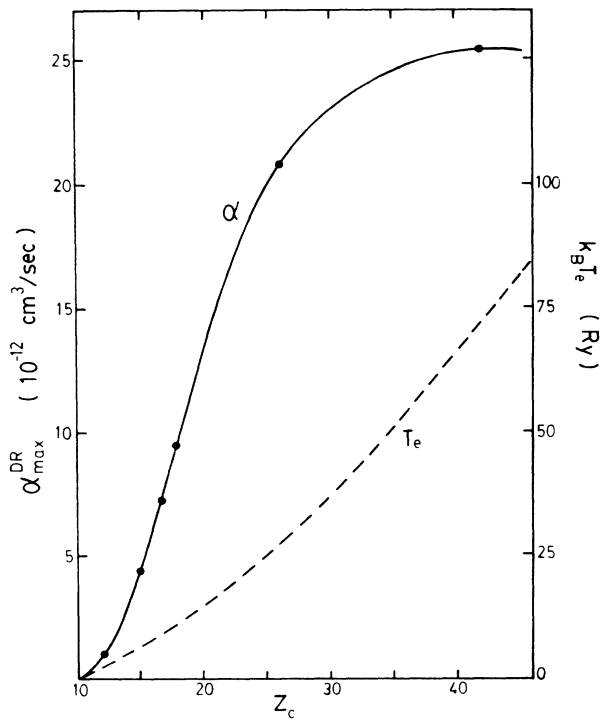

FIG. 3. α^{DR} vs (Z_c) for ten-electron ions "Mg^{2+}, P^{5+}, Cl^{7+}, Ar^{8+}, Fe^{16+}, and Mo^{32+}" in units of 10^{-12} $cm^3\,sec^{-1}$. The maximum rates were chosen in this plot, rather than the rates at scaled temperature which are less realistic for ions with small Z_c. The corresponding electron temperatures T_e at which the rates are maximum are also shown.

IV. CONCLUSION

We explicitly evaluated the DR cross sections and rate coefficients for the Mg^{2+} and P^{5+} target ions, and reevaluated much of the dominant contributions in Cl^{7+}. The state-by-state comparison of the cross sections for different ions was made difficult because of the often drastically shifting character of the Auger widths, accompanied by often drastic reduction in cross sections as the intermediate states are reclassified for different ions. The high-n extrapolation was also very sensitive to this. Although the overall $S(P^{5+})$ is in qualitative agreement with the preliminary data, much more detailed measurements are needed to critically test the theory.

On the other hand, the dielectronic recombination rate coefficients α^{DR} for the ten-electron ions (six ionic species) show a smooth curve from which rate coefficients can be deduced for ten-electron ions lying between Na^{1+} and Mo^{32+}. At very low temperatures (e.g., cold plasma) the DR rate coefficients increase as Z_c decreases, although at higher temperatures the peaks of the rates increase with Z_c.

ACKNOWLEDGMENTS

One of us (A.H.M.) is grateful to the Fulbright Commission for a grant, which made this collaboration possible, and also to the University of Connecticut Research Foundation for partial support. This work was supported in part by a U. S. Department of Energy grant. We benefited from many conversations with Dr. P. Dittner, Dr. P. Miller, and Dr. S. Datz concerning their experiment on P^{5+} and Cl^{7+}. H. H. R. was supported by the Egyptian channeling program.

APPENDIX

We give in Table II sample values of A_a and A_r which are used to calculate the DR cross sections and rate coefficients. They can also be used to evaluate the resonance contribution to collisional excitations, as shown in Eq. (6). Allowed values of Auger transition probabilities A_a and radiative transition probabilities A_r are calculated using the single-configuration nonrelativistic Hartree-Fock approximation in LS coupling. The energy-averaged cross section is given, from Eqs. (2) and (4), as

$$\bar{\sigma}^{DR} = \frac{4\pi\tau_0}{e_c(\mathrm{Ry})}(\pi a_0^2) V_a \omega \frac{1}{\Delta e_c(\mathrm{Ry})} . \quad \text{(A1)}$$

To illustrate, we consider the intermediate state

TABLE II. The cross section σ^{DR} for P^{5+} in units of 10^{-20} cm^2, $\Delta e_c = 0.1$ Ry, and the energies in Ry for the states $3s3p$, $3p^2$, and $3d^2$ are 5.57, 6.50, and 8.75, respectively.

L	S	L_{ab}	S_{ab}	A_a	A_r	A_r	ω	V_a	σ^{DR}
					$3s3p$				
0	0.5	1	0	0.142 + 15	0.126 + 11	0.160 + 10	0.000 099 9	0.142 + 15	0.0683
0	0.5	1	1	0.213 + 15	0.379 + 11		0.000 178	0.213 + 15	0.182
2	0.5	1	0	0.192 + 12	0.126 + 11	0.160 + 10	0.0689	0.960 + 12	0.318
2	0.5	1	1	0.895 + 11	0.379 + 11		0.2975	0.449 + 12	0.643
									1.21
					$3p^2$				
1	0.5	0	0	0.340 + 14		0.345 + 10	0.0001	0.102 + 15	0.035
1	0.5	1	1	0.185 + 15		0.345 + 10	0.000 02	0.555 + 15	0.038
1	0.5	2	0	0.128 + 15		0.345 + 10	0.000 03	0.384 + 15	0.040
3	0.5	2	0	0.460 + 13		0.345 + 10	0.0007	0.322 + 14	0.077
									0.190
					$3d^2$				
1	0.5	0	0	0.592 + 13	0.570 + 11	0.878 + 10	0.011	0.178 + 14	0.599
1	0.5	1	1	0.729 + 13	0.386 + 12	0.878 + 10	0.0514	0.219 + 14	3.448
1	0.5	2	0	0.589 + 13	0.100 + 12	0.878 + 10	0.0181	0.177 + 14	0.981
3	0.5	2	0	0.129 + 14	0.816 + 10	0.878 + 10	0.0013	0.903 + 13	0.0362
3	0.5	3	1	0.337 + 14	0.171 + 12	0.878 + 10	0.0053	0.236 + 15	3.838
3	0.5	4	0	0.859 + 14	0.220 + 12	0.878 + 10	0.0027	0.601 + 15	4.896
5	0.5	4	0	0.256 + 13		0.878 + 10	0.0034	0.282 + 14	0.295
									14.1

$1s^2 2s^2 2p^5 3s3p$ in the reaction

$$1s^2 2s^2 2p^6 + e_c l_c \rightarrow (1s^2 2s^2 2p^5 3s3p)LS \rightarrow 1s^2 2s^2 2p^6 3p + \gamma \ . \quad \text{(A2)}$$

The particular coupling order we adopted[1] gives

$$[2p^5, (3s3p)L_{ab}S_{ab}]LS \ ,$$

with $L_{ab}=1$ and $S_{ab}=0$ and 1. This in turn gives $L=0$, 1, and 2 and $S=\frac{1}{2}$ and $\frac{3}{2}$. However, parity conservation excludes the state with $L=1$. The quartet state with $S=\frac{3}{2}$ is not present in the reaction (A2), by spin conservation. Among the dominant intermediate states are $2p^5 3dnd$ followed by $2p^5 3pnd$ and $2p^5 3dnf$.

From Table II, we can also estimate the resonance contribution to elastic scattering (RS) using Eq. (6). From Eq. (2), however, we simply have in these cases tabulated in Table II,

$$\sigma^{RS} = \sigma^{DR}(1-\omega)/\omega \ ,$$

with the Auger yield $\zeta \equiv 1-\omega$. Again, using $\Delta e_c = 0.1$ Ry, we obtain

$$\sigma^{RS}(i \rightarrow 3s3p) = 1.71 \times 10^{-17} \text{ cm}^2 \ ,$$
$$\sigma^{RS}(i \rightarrow 3p^2) = 3.10 \times 10^{-17} \text{ cm}^2 \ ,$$
$$\sigma^{RS}(i \rightarrow 3d^2) = 2.83 \times 10^{-17} \text{ cm}^2 \ .$$

They are to be compared with

$$\sigma^{DR}(i \rightarrow 3s3p) = 1.21 \times 10^{-20} \text{ cm}^2 \ ,$$
$$\sigma^{DR}(i \rightarrow 3p^2) = 0.19 \times 10^{-20} \text{ cm}^2 \ ,$$
$$\sigma^{DR}(i \rightarrow 3d^2) = 14.1 \times 10^{-20} \text{ cm}^2 \ .$$

There is an overall factor of approximately 10^3 between the RS and DR cross sections.

[1] Y. Hahn, Adv. At. Mol. Phys. **21**, 123 (1985).

[2] D. S. Belic, G. H. Dunn, T. J. Morgan, D. W. Mueller, and C. Timmer, Phys. Rev. Lett. **50**, 339 (1983); A. Mueller *et al.*, *ibid.* **56**, 127 (1986).

[3] B. A. Mitchell *et al.*, Phys. Rev. Lett. **50**, 335 (1983).

[4] P. F. Dittner, S. Datz, P. D. Miller, P. L. Pepmiller, and C. M. Fou, Phys. Rev. A **33**, 124 (1986).

[5] J. F. Williams, Phys. Rev. A **29**, 2936 (1984).

[6] K. LaGattuta and Y. Hahn, Phys. Rev. Lett. **51**, 558 (1983); K. LaGattuta, I. Nasser, and Y. Hahn, Phys. Rev. A **33**, 2782 (1986).

[7] J. A. Tanis *et al.*, Phys. Rev. Lett. **49**, 1325 (1982); **53**, 2551 (1984); E. M. Bernstein *et al.*, Nucl. Instrum. Methods **24/25**, 232 (1987).

[8] M. Clark, D. Brandt, J. K. Swenson, and S. M. Shafroth, Phys. Rev. Lett. **54**, 544 (1985).

[9]M. Schulz *et al.*, Phys. Rev. Lett. **58**, 1734 (1987).
[10]C. Breton *et al.*, Phys. Rev. Lett. **41**, 110 (1978).
[11]M. Bitter *et al.*, Phys. Rev. Lett. **43**, 129 (1979).
[12]J. S. Wang, H. R. Griem, R. Hess, W. F. Rowan, and T. P. Kochanski, Phys. Rev. A **33**, 4293 (1986).
[13]J. P. Briand *et al.*, Phys. Rev. Lett. **52**, 617 (1984).
[14]P. Dittner *et al.* (private communication).
[15]K. LaGattuta and Y. Hahn, Phys. Rev. A **26**, 1125 (1982).
[16]Y. Hahn, J. N. Gau, G. Omar, and M. P. Dube, Phys. Rev. A **36**, 576 (1987).
[17]J. N. Gau, Y. Hahn, and J. A. Retter, J. Quant. Spectrosc. Radiat. Transfer **23**, 147 (1980).
[18]M. Chen, Phys. Rev. A **34**, 1073 (1985).
[19]Y. Hahn, J. N. Gau, and J. A. Retter, J. Quant. Spectrosc. Radiat. Transfer **23**, 65 (1980).